Editors' Suggestion

Edge states and topological pumping in stiffness-modulated elastic plates

Emanuele Riva,[1] Matheus I. N. Rosa,[2] and Massimo Ruzzene[3]
[1]*Department of Mechanical Engineering, Politecnico di Milano, Milano 20156, Italy*
[2]*School of Mechanical Engineering, Georgia Institute of Technology, Atlanta, Georgia 30332, USA*
[3]*Department of Mechanical Engineering, University of Colorado Boulder, Boulder, Colorado 80309, USA*

(Received 19 November 2019; revised manuscript received 2 March 2020; accepted 3 March 2020; published 23 March 2020)

We demonstrate that modulations of the stiffness properties of an elastic plate along a spatial dimension induce edge states spanning nontrivial gaps characterized by integer-valued Chern numbers. We also show that topological pumping is induced by smooth variations of the phase of the modulation profile along one spatial dimension, which results in adiabatic edge-to-edge transitions of the edge states. The concept is first illustrated numerically for sinusoidal stiffness modulations and then experimentally demonstrated in a plate with square-wave thickness profile. The presented numerical and experimental results show how continuous modulations of properties may be exploited in the quest for topological phases of matter. This opens new possibilities for topology-based waveguiding through slow modulations along a second dimension, spatial or temporal.

DOI: 10.1103/PhysRevB.101.094307

I. INTRODUCTION

The search for topological phases of matter has reached a mature state with multiple realizations across different physical realms, including quantum [1], electromagnetic [2,3], acoustic [4–6], and elastic [7] media. In mechanics, topologically protected wave transport has been demonstrated through analogs to the *quantum Hall effect* (QHE) [8–15], the *quantum spin Hall effect* (QSHE) [7,16–20], and the *quantum valley Hall effect* (QVHE) [21–24]. The rich underlying physics makes these robust waveguiding mechanisms promising for applications in acoustic devices or structural components designed to steer waves or isolate vibrations.

Recently, topological phases have been explored in systems of lower physical dimensions by exploiting synthetic dimensions emerging from the exploration of relevant parameter spaces [25–28]. Notable examples include the observation of edge states, commonly attributed to two-dimensional (2D) QHE systems, in 1D quantum [29], electromagnetic [30], acoustic [31,32], and mechanical [33–35] lattices following the Aubry-André-Harper model of interactions [36,37]. Also, 4D quantum Hall phases have been realized using 2D photonic lattices [38] and ultracold atoms [39], while 6D phases in 3D systems have been theoretically investigated in Refs. [28,40]. In this context, topological pumping has been pursued in a variety of physical systems, whereby adiabatic transitions of edge states are induced by smooth parameter variations along spatial [30,34,38,39,41] or temporal [15,42–46] dimensions. While previous experimental studies demonstrate pumping in photonic lattices and cold atomic gases, a realization using elastic waves is currently missing.

In the quest for topological phases of matter, elastic solids such as thin, elastic plates are promising platforms due to the convenience they offer in terms of manufacturing and testing, and their rich spectral properties which are characterized by a large number of wave modes of distinct polarizations [20]. At the same time, the abundance of polarizations makes implementing topological waveguiding in elastic plates a challenging and nontrivial development, when compared to acoustic [4] and electromagnetic [2,3] counterparts. Toward overcoming these challenges and expanding the range of possibilities for topology-based elastic waveguiding, topological pumping is here experimentally demonstrated for the first time in a continuous elastic plate. The investigations herein leverage prior work on discrete lattices of continuous elastic waveguides [34] whereby modulations of physical properties along a spatial dimension were shown to induce edge states spanning nontrivial gaps. Smooth phase variations of the modulation profile along a second spatial dimension induce transitions of the edge modes from being localized at one boundary, to a bulk mode, and, finally, to a localized mode at the opposite boundary. In here, harmonic stiffness modulation profiles are first investigated to illustrate pumping numerically. Square-wave thickness modulations are then employed in the experimental demonstration of the concept. While the majority of studies has so far focused on discrete lattice systems, our results provide a general strategy to achieve topological pumping through continuous property modulations and open new paths toward exploring higher-dimensional topological phases exploiting higher dimensions in continuous systems.

II. ANALAYSIS OF EDGE STATES AND TOPOLOGICAL PUMPING IN MODULATED PLATES

We consider elastic plates characterized by a bending stiffness which is periodically modulated along the x direction, i.e., $D(x, y) = D(x + \lambda_m, y)$, where λ_m is the modulation wavelength. Two configurations are investigated in this work (Fig. 1). The first one employs a conceptual harmonic stiffness modulation of the form

$$D(x, y) = D_0\{1 + a_m \cos[\kappa_m x + \phi(y)]\}, \tag{1}$$

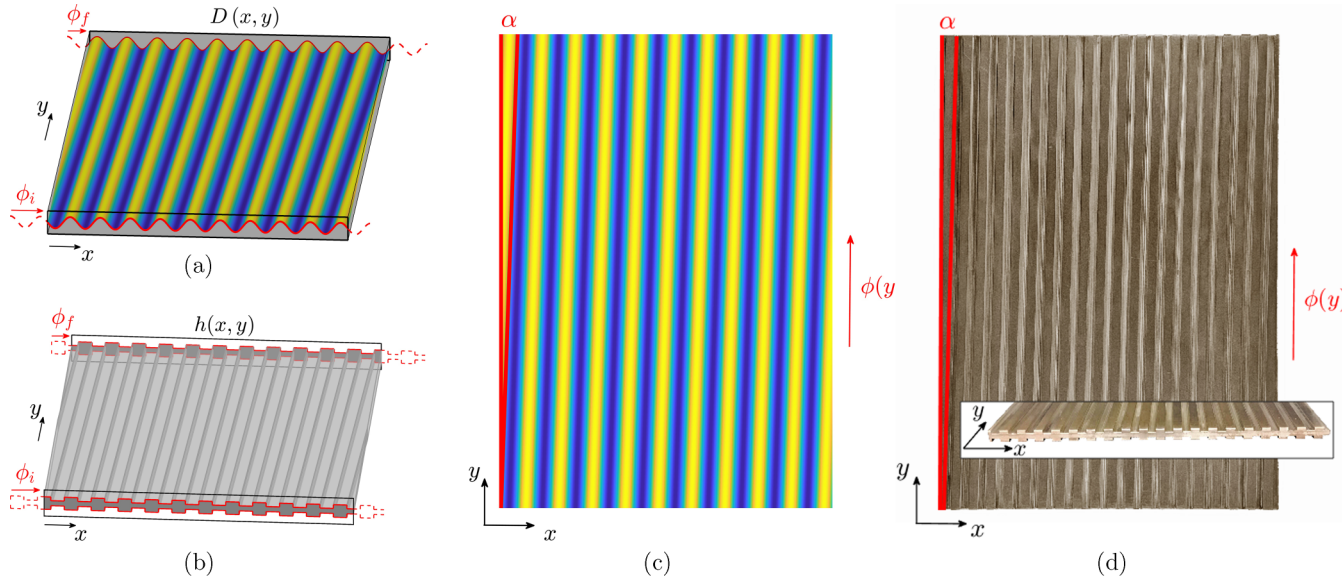

FIG. 1. Stiffness modulations and plate configurations. (a) Plate (shaded gray solid) characterized by a harmonic stiffness modulation $D(x, y) = D_0\{1 + a_m \cos[\kappa_m x + \phi(y)]\}$ (colored surface). The schematic illustrates a linear phase change from ϕ_i to ϕ_f. (b) Schematic of plate with square-wave modulation of thickness $h(x, y) = h_0(1 + a_m \operatorname{sgn}\{\cos[\kappa_m x + \phi(y)]\})$. The phase also varies linearly from ϕ_i to ϕ_f. (c) Top view of modulation in (a) illustrating the shift of the profile characterized by a tilting angle α. (d) Top view and perspective view (inset) of square wave modulated plate employed in experiments. The sample is characterized by parameters $\lambda_m = 1.6$ cm, $h_0 = 4.7$ cm, $a_m = 0.38$, $L_x = 31.2$ cm, and $L_y = 43.7$ cm and phase varying linearly from $\phi_i = 0.7\pi$ to $\phi_f = -0.7\pi$.

where $\kappa_m = 2\pi/\lambda_m$, while a_m and ϕ, respectively, denote amplitude and phase of the modulation. The phase $\phi(y)$ determines the stiffness value $D(0, y)$ at the left boundary of the plate. If smoothly varied along y, then it produces the tilted modulation profile shown in Figs. 1(a) and 1(c). This choice follows previous work where sinusoidal modulations define the coupling within continuous waveguides in the context of topological adiabatic pumping [34].

The second configuration corresponds to a thickness profile $h(x, y)$ described by a square wave of the form [Fig. 1(b)]:

$$h(x, y) = h_0(1 + a_m \operatorname{sgn}\{\cos[\kappa_m x + \phi(y)]\}), \tag{2}$$

which produces a periodic modulation of the plate bending stiffness according to the expression $D(x, y) = Eh(x, y)^3/[12(1 - \nu^2)]$, where E, ν are respectively the Young's modulus, and the Poisson's ratio of the plate material. This choice is driven by fabrication considerations in the experimental activities of this work.

The effects of the harmonic stiffness modulation [Eq. (1)] are investigated analytically by considering Kirchhoff-Love's plate theory [47]. According to the theory, the harmonic motion at frequency ω, $w(x, y, \omega)$, in the direction perpendicular to the plate plane x, y is governed by the following equation of motion:

$$\begin{aligned}&[D(w_{,xx} + \nu w_{,yy})]_{,xx} + 2[(1 - \nu)Dw_{,xy}]_{,xy} \\ &\quad + [D(w_{,yy} + \nu w_{,xx})]_{,yy} = \omega^2 m w,\end{aligned} \tag{3}$$

where $()_{,q}$ denotes a partial derivative with respect to q and $m = \rho h$ is the mass density. We investigate the dispersion properties of the plate $\omega = \omega(\kappa_x, \kappa_y, \phi)$, where the phase modulation ϕ is explicitly denoted as a free parameter. To this end, we impose plane-wave solutions $w(x, y) = w(x)e^{j\kappa_y y}$, where $w(x) = \sum_n \hat{w}_n e^{j(\kappa_x + n\kappa_m)x}$, $n = -N, \ldots, +N$ reflects the x-wise periodicity of the plate. Application of the plane-wave expansion method (PWEM) (see Supplemental Material [48]), leads to an eigenvalue problem in the form:

$$\boldsymbol{K}(\kappa_x, \kappa_y, \phi)\hat{\boldsymbol{w}} = m\omega^2 \hat{\boldsymbol{w}}, \tag{4}$$

where $\boldsymbol{K}$ is the $N \times N$ stiffness matrix and $\hat{\boldsymbol{w}} = \{\hat{w}_{-N}, \ldots, \hat{w}_N\}^T$. Solution of the eigenvalue problem in Eq. (4) yields the dispersion properties, described in terms of eigenvalues ω_i and associate wave modes w_i defined by the components of the eigenvector $\hat{\boldsymbol{w}}_i$.

We begin our study by evaluating dispersion along x for assigned values of κ_y. Results for $\kappa_y = 0$, shown in Fig. 2(a), correspond to letting $()_{,y} = 0$ in Eq. (3), which yields an expression akin to the equation governing the transverse motion of 1D elastic Euler Bernoulli beams [49]. In Fig. 2(a), $\mu_x = \kappa_x \lambda_m$, while $\Omega = \omega/\omega_0$ is a nondimensional frequency, with $\omega_0 = \kappa_m^2\sqrt{D_0/m}$. The results, obtained for $a_m = 0.8$, effectively correspond to the dispersion characteristics of a family of 1D, decoupled elastic beams characterized by stiffness modulations that differ by the phase parameter ϕ. The dispersion eigenvalues feature two bands separated by a gap that remains constant with ϕ. Indeed, continuous shifts of the stiffness along x can be interpreted as a translation of the λ_m-periodic unit cell along x, which does not affect the eigenfrequencies. However, these shifts do affect the eigenvectors, as it is revealed by the analysis of the topology of the bands. Such analysis relies on the evaluation of band's Chern number in the $(\mu_x, \phi) \in \mathbb{T}^2 = [0, 2\pi] \times [0, 2\pi]$ space [34,50], which is given by

$$C = \frac{1}{2\pi i}\int_{\mathcal{D}} \nabla \times (w_i^* \cdot \nabla w_i)\, d\mathcal{D}, \tag{5}$$

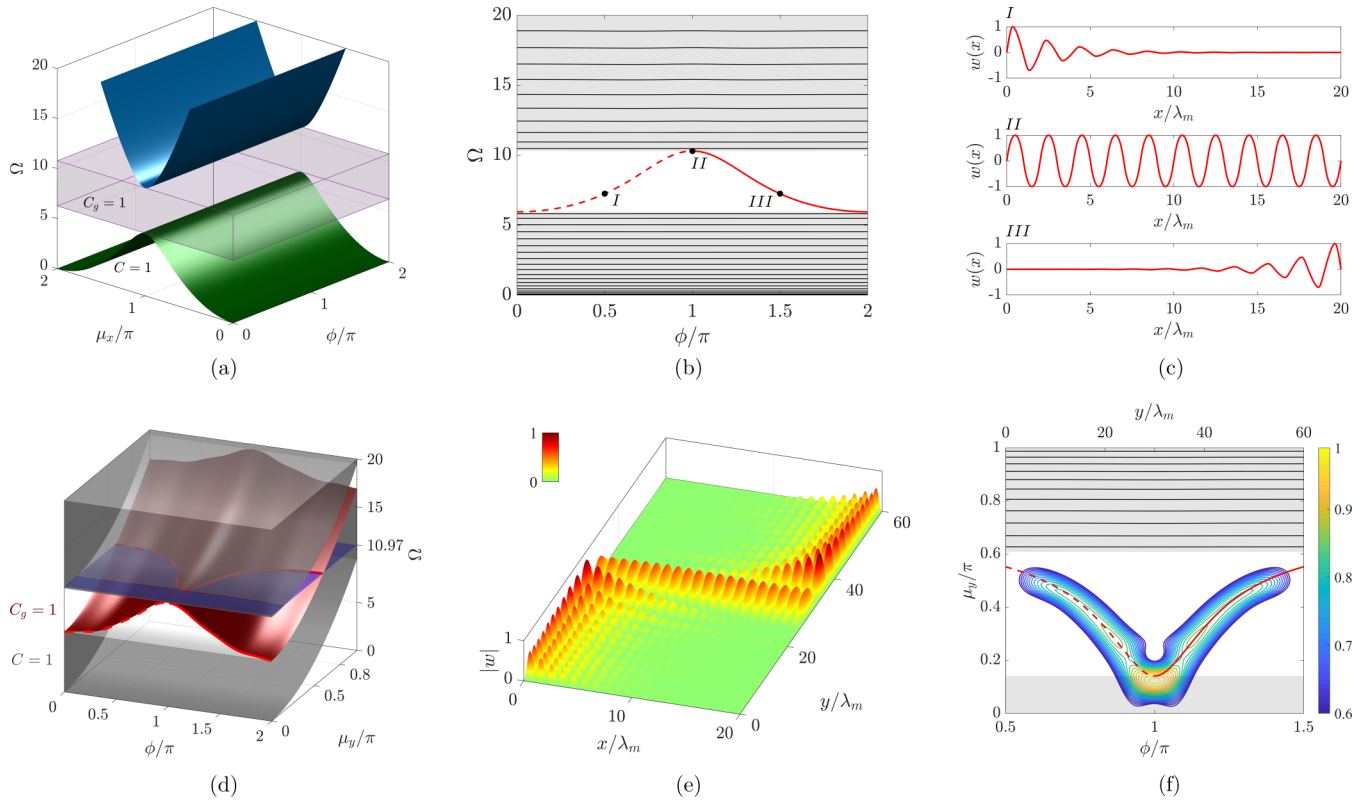

FIG. 2. Dispersion properties and topological pumping for elastic plate with harmonic stiffness modulation $D(x, y) = D_0\{1 + a_m \cos[\kappa_m x + \phi(y)]\}$. (a) Dispersion surfaces $\Omega(\mu_x, \phi)$ for $\mu_y = 0$ showing two bands separated by a gap, with information on Chern numbers and gap label. (b) Frequency spectrum of the finite plate with $L_x = 20\lambda_m$ and $\mu_y = 0$ as a function of ϕ: Black straight lines corresponding to finite structure modes are superimposed to the bulk bands (shaded gray regions), while an edge mode (red curve) spans the gap. (c) Representative left-localized, bulk, and right-localized modes corresponding to the points marked in (b). (d) Variation of the finite plate spectrum in (b) as a function of μ_y. The red surface represents the dispersion of the edge state, while shaded gray volumes are the bulk bands. The red line at $\mu_y = 0$ highlights the transition of the edge state from left-localized (dashed) to right localized (solid) at $\phi = \pi$. (e) Steady-state response $|w(x, y)|$ of the modulated plate at frequency $\Omega = 10.97$, where the associated colormap also represents normalized displacement. Topological pumping occurs through a transition of the edge state from left localized ($\phi_i = 0.5\pi$) to right localized ($\phi_f = 1.5\pi$) due to the phase modulation $\phi(y) = \phi_i \to \phi_f$. (f) Cross section of dispersion diagram in (d) at frequency $\Omega = 10.97$ as a function of $\phi \in [0.5\pi, 1.5\pi]$. Black (straight) lines and red curves, respectively, denote bulk and edge modes of the finite plate. The contours of the spectrogram of the displacement field $|\hat{w}(y, \mu_y)|$ reveal that pumping occurs through a transition along the wave-number branch of the edge state.

where $\mathcal{D} = \mathbb{T}^2$, $\boldsymbol{\nabla} = (\partial/\partial\mu_x)\boldsymbol{e}_{\mu_x} + (\partial/\partial\phi)\boldsymbol{e}_\phi$, and $()^*$ denotes a complex conjugate. The Chern number is evaluated numerically over a discretized (μ_x, ϕ) space according to the procedure described in Ref. [51], which gives the label assigned to the first band in Fig. 2(a). A label for a gap r is then assigned by computing the algebraic sum of the Chern numbers of the bands below it [34,50], i.e., $C_g^{(r)} = \sum_{n=1}^{r} C_n$, which yields $C_g = 1$ for the gap considered in Fig. 2(a). In finite structures, a nonzero gap label signals the presence of topological edge states spanning the associated gap as a result of a parameter sweep. The existence of an edge state as ϕ varies in the $[0,\ 2\pi]$ range is verified by computing the spectral properties of a plate bounded along the x direction, which are evaluated by constructing an eigenvalue problem similar to that of Eq. (4), where a solution of the kind $w(x, y) = e^{j\kappa_y y} \sum_n \hat{w}_n \sin(\frac{n\pi x}{L_x})$, $n = 1, \ldots, N$ is imposed to satisfy the conditions at the plate x boundaries, i.e., $w(x = 0, L_x; y) = w_{,xx}(x = 0, L_x; y) = 0$ [48]. Figure 2(b) shows the modes of a finite plate of length $L_x = 20\lambda_m$ as a function of ϕ for $\kappa_y = 0$. The modes (black straight lines) belonging to the bulk bands, which are shown for reference as the shaded gray regions, do not vary as a function of ϕ. An additional mode (red line) traversing the gap and varying with ϕ corresponds to a topological edge state localized at either the left or right boundary depending on the value of ϕ, with the right (left) localization of the mode being denoted by the solid (dashed) red line. The transition of the edge state with variations of ϕ is related to the gap label $C_g = 1$. In particular, its absolute value $|C_g| = 1$ indicates that the edge state traverses the gap once for $\phi \in [0, 2\pi]$, while its positive sign relates to a left-to-right transition that occurs when the branch of the edge state touches the upper boundary of the gap at $\phi = \pi$. Representative left-localized (point I) and right-localized modes (point III) are displayed in Fig. 2(c), along with the mode extending to the bulk in correspondence to the branch touching the bulk band (point II). These observations are in agreement with the behavior of edge states and their correspondence to the gap labels in discrete lattices [34,50].

Next, we discuss the dispersion properties for values $\kappa_y \neq 0$. These values do not affect the structure of the eigenvalue problem in Eq. (4) and only introduce a frequency shift. This is illustrated in Fig. 2(d), which displays the dispersion of a modulated plate with $a_m = 0.8$. Since the dispersion relations here are functions of three parameters $\Omega(\mu_x, \mu_y, \phi)$, their graphical interpretation is problematic. In the plot under consideration, we represent the range spanned by the dispersion relations for $\mu_x \in [0, \pi]$ by the shaded gray volumes. The bands variation in terms of μ_y and ϕ illustrates the preservation of the gap at frequencies that increase monotonically with μ_y. The modes of a finite plate with $L_x = 20\lambda_m$ populate these bulk bands, here omitted for simplicity, and also include a mode spanning the gap, which is represented by the red surface in the figure. The red lines superimposed at $\mu_y = 0$ illustrate the transition experienced by the edge state as in Fig. 2(b), which now occurs as a function of μ_y along the entire surface of the edge state. We verify that the topological properties are preserved with μ_y by computing the Chern number C for distinct, fixed μ_y values. To this end, we consider the $(\mu_x, \phi) \in \mathbb{T}^2 = [0, 2\pi] \times [0, 2\pi]$ space to compute the gap labels in Fig. 2(d) for the probed μ_y values. Since C_g is invariant with μ_y, the occurrence of the edge state (represented by the red surface) is observable in the entire (μ_y, ϕ) space.

The transitions of the edge states can be exploited to implement a topological pump that employs an adiabatic (slow) variation of ϕ along a second dimension [30,34,44,52]. For a finite plate of length L_y, we consider a smooth, linear phase modulation of the kind $\phi(y) = \phi_i(1 - \frac{y}{L_y}) + \phi_f \frac{y}{L_y}$ [Fig. 1(a)]. A top view of a representative harmonic stiffness modulation is displayed in Fig. 1(c), where a positive tilting angle $\alpha = \tan^{-1}[-(\phi_f - \phi_i)/(\kappa_m L_y)]$ resulting from a choice with $\phi_i > \phi_f$ is illustrated. We first demonstrate topological pumping numerically by considering a plate with $L_y = 3L_x$ and phase variation with $\phi_i = 0.5\pi$ and $\phi_f = 1.5\pi$. Similarly to prior work [30,34], the chosen interval $\phi \in [0.5\pi, 1.5\pi]$ exploits a restricted portion of the branch of the edge state whereby a single transition from the left boundary ($\phi_i = 0.5\pi$) to the right boundary ($\phi_f = 1.5\pi$) is induced. This is in contrast with alternative experimental realizations where several pumping cycles are induced through periodic property modulations [42,43]. To verify this, we compute the forced response of the plate when harmonically excited by a distributed force per unit area $q(x, y, t) = f(x)\delta(y - y_e)e^{i\omega t}$. The force is applied near the bottom boundary ($y_e = \lambda_m/2$) and has a spatial distribution $f(x)$ that corresponds to the left-localized edge state obtained for $\phi_i = 0.5\pi$ [see Mode I in Fig. 2(c)]. This favors the excitation of the desired topological mode, while minimizing the contribution from bulk modes coexisting at the same frequency. The response of the plate is evaluated through a Galerkin [49] approximation of the displacement field $w(x, y)$, similarly to that employed to obtain the modes of the finite plate (see details in the Supplemental Material [48]). The response of the plate for an excitation frequency of $\Omega = 10.97$ [Fig. 2(e)] consists of a topological pump whereby energy is transferred from the bottom left boundary to the upper right boundary of the plate via an edge state transition. Additional examples are reported in the Supplemental Material [48]. The topological pumping results from an adiabatic evolution along the wave-number branch of the edge state at a given frequency [34], which is illustrated for the pump of Fig. 2(e) by considering a cross section of the dispersion diagram at frequency $\Omega = 10.97$ [blue plane in Fig. 2(d)]. The results in Fig. 2(f) are displayed for $\phi \in [0.5\pi, 1.5\pi]$, which is the interval considered for the phase modulation $\phi(y)$. Shaded gray areas correspond to the intersection between the blue plane and the bulk bands (shaded gray volumes) of Fig. 2(d) and represent the dispersion $\mu_y(\Omega = 10.97, \phi)$ obtained from the projection of the bands occupied for $\mu_x \in \{0, \pi\}$. These bands are populated by modes of the finite plate with $L_x = 20\lambda_m$ (black straight lines), while the intersection between the blue plane and the red surface in Fig. 2(d) defines the edge state (red line) that spans the gap as a function of ϕ. The previously described forcing profile selectively excites the left-localized edge state (for $\phi_i = 0.5\pi$) at the bottom boundary of the plate, while a smooth phase modulation $\phi(y) = \phi_i \to \phi_f$ drives the left-to-right transition of the edge state along y, which occurs along the branch defined by the red curves in Fig. 2(f). We verify such a transition by computing 2D Fourier transforms (FT) while performing an appropriate windowing of the displacement field to capture wave-number changes along y. The procedure consists on premultiplying the displacement field $w(x, y)$ by a Gaussian window centered at $y = y_0$, i.e., $G(x, y) = e^{-(y-y_0)^2/2c^2}$, where c is a parameter controlling the Gaussian's width. A FT operation then quantifies the displacement field in reciprocal space $\hat{w}(y_0, \mu_x, \mu_y)$ around the location $y = y_0$. The dependence of μ_x is then eliminated by taking the L^1 norm along μ_x, which produces $\hat{w}(y, \mu_y)$. The corresponding spectrogram, obtained for $c = 0.07$, is displayed in the form of contour plots in Fig. 2(f), where the colors represent the normalized magnitude of the displacement field $|\hat{w}(y, \mu_y)|$. The procedure confirms that energy remains concentrated on the wave-number branch of the edge state according to the modulation $\phi(y)$, which characterizes the topological pump displayed in Fig. 2(e).

III. EXPERIMENTAL OBSERVATION OF TOPOLOGICAL PUMPING IN SQUARE-MODULATED PLATE

Topological pumping is experimentally demonstrated in a plate with square-wave thickness modulation $h(x, y) = h_0(1 + a_m \operatorname{sgn}\{\cos[\kappa_m x + \phi(y)]\})$ with modulation parameters $\lambda_m = 1.6$ cm, $h_0 = 4.7$ cm, $a_m = 0.38$, $\phi_i = 0.7\pi$, and $\phi_f = -0.7\pi$ [Fig. 1(b)]. The plate is rectangular of dimensions 31.2 cm × 43.7 cm, and it is made of aluminum [Fig. 1(d)]. A linear phase modulation produces the tilted thickness profile in Fig. 1(d).

The plate dispersion properties are computed using a finite-element (FE) model implemented in the COMSOL MULTIPHYSICS environment [48]. The computations provide information on all wave modes, whose polarizations are tracked by computing a polarization factor [20] that quantifies the relationship between in-plane (u, v) and out-of-plane (w) components of the displacement field. The polarization factor is employed to discriminate and isolate out-of-plane polarized wave modes, which are weakly coupled to the in-plane ones. We compare the results to experimental data consisting of the out-of-plane velocity field $\dot{w}(x, y, t)$ of the plate's surface

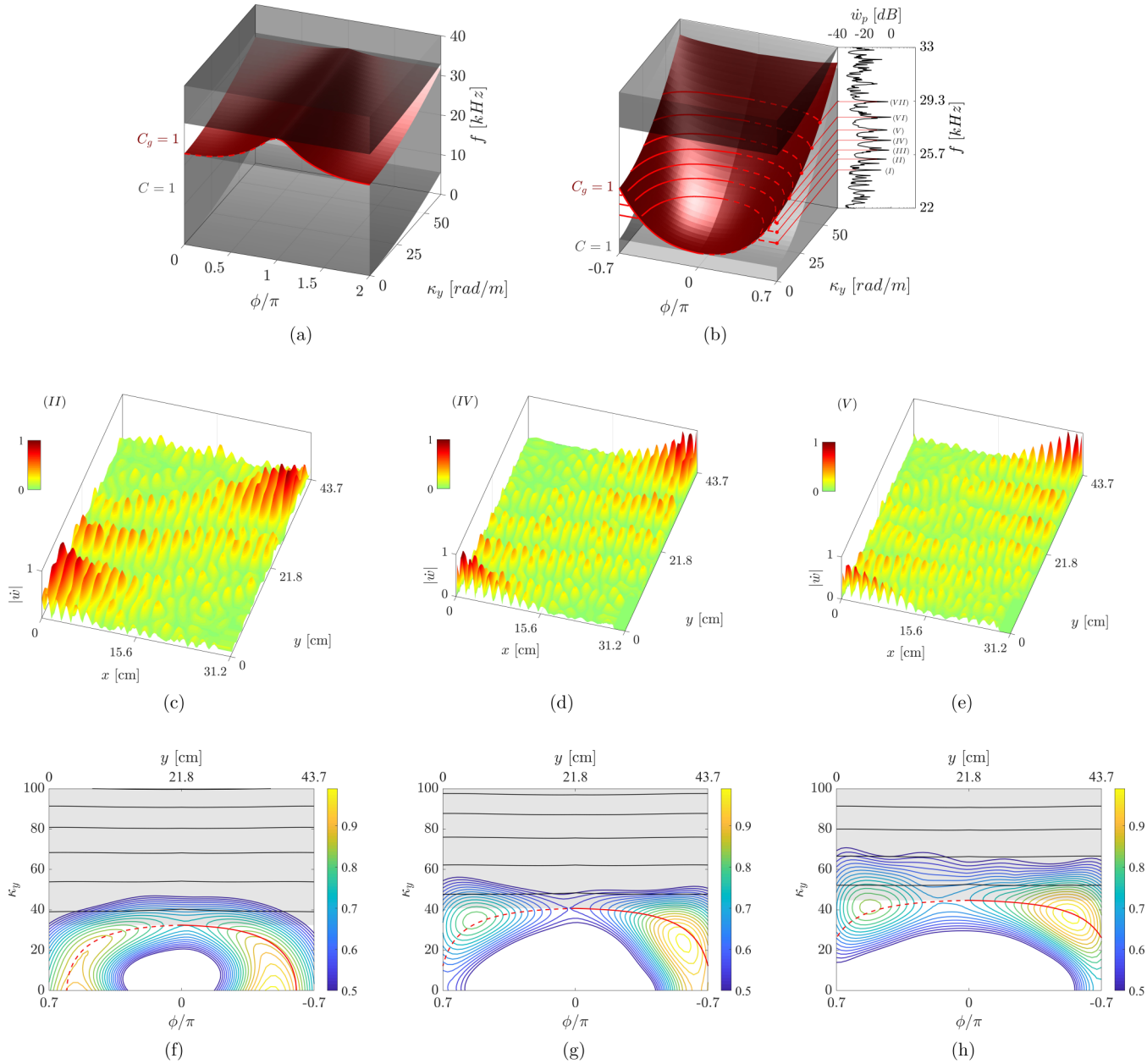

FIG. 3. Dispersion properties and experimental observation of topological pumping in plate with square-wave modulation of the thickness $h(x, y) = h_0(1 + a_m \,\mathrm{sgn}\{\cos[\kappa_m x + \phi(y)]\})$. (a) Dispersion properties and edge state (red surface) for a finite plate with $L_x = 31.2$ cm and free-free boundary conditions along x. Bulk bands are represented by shaded gray volumes, along with Chern number and gap labels information. (b) Detail of dispersion for $\phi \in [-0.7\pi, 0.7\pi]$, corresponding to the interval considered for the phase modulation of thickness. The experimentally measured frequency response spatially averaged over the plate surface is displayed alongside the dispersion. Each resonant peak defines a wave-number branch highlighted by dashed and solid red lines in the dispersion surface, along which topological pumping occurs at the corresponding frequency. [(c)–(e)] Experimentally measured velocity field $|\dot{w}(x, y)|$ for selected resonant peaks II, IV, and V. The transitions from localization at the left boundary to localization at the right boundary that characterize topological pumping are quantified by the spectrograms displayed in (f)–(h), which confirm that energy is concentrated around the wave-number branches of the edge states.

measured by a scanning laser Doppler vibrometer (see details in the Supplemental Material [48]).

The numerically computed dispersion relations are shown in Fig. 3(a), where, as previously, the red surface corresponds to the edge state, while the shaded gray volumes denote the bulk bands. Similarly to the case of harmonic modulation, the existence of an edge state spanning the gap is associated with the nontrivial band topology identified by integer-valued Chern numbers. Chern numbers and gap labels are numerically evaluated using the Bloch modes obtained through the FE model according to the procedure outlined in the Supplemental Material [48], which yields the labels displayed in Fig. 3(a). We find that the first spectral gap produced by the square modulation is also characterized by a gap label $C_g = 1$, which signals a left to right transition of the edge state, again highlighted by the dashed and solid red curves at $\kappa_y = 0$. This

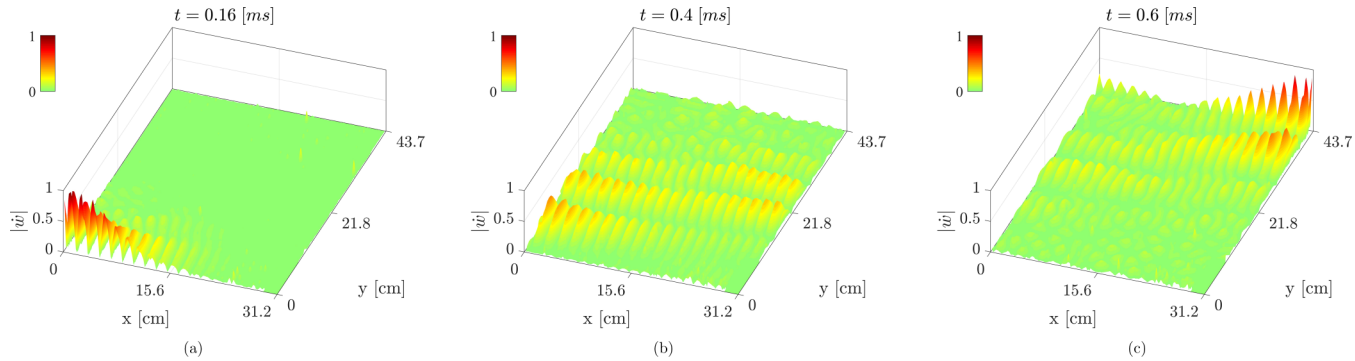

FIG. 4. Experimental observation of transient topological pumping in square-modulated plate. Panels (a)–(c) display snapshots of the measured velocity field for three subsequent time instants, where the transition from left-localized (a), to bulk (b), and, finally, to right-localized mode (c) as the wave propagates along y can be observed.

transition occurs at $\phi = \pi$ along the entire surface of the edge state, which is consistent with constant-valued Chern numbers evaluated as a function of κ_y in the considered frequency range ($f \in [0, 40]$ kHz). Figure 3(b) displays a zoomed view of the dispersion in Fig. 3(a) for $\phi \in [-0.7\pi, 0.7\pi]$, with the observation that the interval $[-0.7\pi, 0]$ coincides with $[1.3\pi, 2\pi]$ due to the periodicity with ϕ. This interval corresponds to the phase modulation of the manufactured plate, i.e., from $\phi_i = 0.7\pi$ to $\phi_f = -0.7\pi$, which exhibits the transition of the edge state occurring at the bottom boundary of the gap.

The experiment is conducted by clamping the plate at its bottom right boundary while excitation is induced by a pair of piezoelectric ceramic patches attached to the bottom left boundary [48]. The patches are connected to opposite electrical poles, which induces an out-of-phase (dipole) excitation that favors the excitation of the left-localized topological mode (for $\phi_i = 0.7\pi$), while reducing the contribution from bulk modes. The forced frequency response function, corresponding to the response spatially averaged over the plate surface, is displayed alongside the dispersion surfaces. The finite size of the plate introduces a series of resonant peaks that are observed in the frequency range within which the edge state exists. At these frequencies, topological pumping is observed through a transition along the wave-number branch of the edge state, as illustrated by the dashed and solid red lines in Fig. 3(b), respectively, denoting left- and right-localized modes. The measured velocity fields for three selected resonant frequencies are displayed in Figs. 3(c)–3(e), where transitions from left to right localization characterizing the pump can be observed. For each of those recorded responses, a spectrogram is computed as described in Sec. II and displayed in Figs. 3(f)–3(h), which confirms the transition along the wave-number branch corresponding to the edge state. We remark that for the first peaks, such as in the case reported in Fig. 3(c), the edge state is only defined within a restricted domain of the parameter space. In such cases, pumping still occurs through the wave-number branch of the edge state but is defined in a shorter spatial domain centered at the midportion of the plate, as confirmed by the spectrogram of Fig. 3(f) corresponding to the pump of peak II.

The results reported in Fig. 3 confirm the existence of steady-state topological pumping in the square-modulated plate occurring for several operating frequencies within [25, 30] kHz, while populating the dispersion surface associated with the edge state. The potential of the modulated plate as a waveguiding platform is further demonstrated by realizing topological pumping in a transient regime. To that end, an excitation in the form of a 7-cycle sine burst signal of center frequency $f = 26.7$ kHz is employed, which aims at transporting energy through the pump defined by peak IV in Fig. 3(b). Figure 4 displays the measured velocity wavefield in the modulated plate at three subsequent time instants: a clear transition from left-localized wave [Fig. 4(a)], to bulk wave [Fig. 4(b)], and, finally, to right-localized wave propagation [Fig. 4(c)] is observed consistent with the expected topological pumping behavior. A video animation of the full transient response is provided in the Supplemental Material [48].

IV. CONCLUSIONS

In this paper, we present the first experimental demonstration of topological pumping in continuous elastic plates. We illustrate a simple design principle based on continuous property modulations which can be employed to induce the existence of topological edge states and drive their edge-to-edge transition. Although a simple linear phase modulation was considered in this work, future work may explore the effects of different modulation profiles beyond the liner one considered herein, which may lead to pumping occurring based on different rates and transition modalities along the modulation direction. The results also provide opportunities for exploring higher dimensional physics in mechanics by exploiting synthetic dimensions in parameter space, which can be mapped to real spatial or temporal dimensions. These concepts have implications of technological relevance for applications involving elastic wave manipulation, such as guiding of bulk, surface and guided waves in acoustic devices, ultrasonic imaging, and nondestructive evaluation.

ACKNOWLEDGMENTS

The authors gratefully acknowledge the support from the National Science Foundation through the EFRI 1741685 grant and from the Army Research office through Grant No. W911NF-18-1-0036.

[1] M. Z. Hasan and C. L. Kane, Colloquium: Topological insulators, Rev. Mod. Phys. **82**, 3045 (2010).

[2] L. Lu, J. D. Joannopoulos, and M. Soljačić, Topological photonics, Nat. Photon. **8**, 821 (2014).

[3] A. B. Khanikaev, S. H. Mousavi, W.-K. Tse, M. Kargarian, A. H. MacDonald, and G. Shvets, Photonic topological insulators, Nat. Mater. **12**, 233 (2013).

[4] Z. Yang, F. Gao, X. Shi, X. Lin, Z. Gao, Y. Chong, and B. Zhang, Topological Acoustics, Phys. Rev. Lett. **114**, 114301 (2015).

[5] R. Fleury, A. B. Khanikaev, and A. Alu, Floquet topological insulators for sound, Nat. Commun. **7**, 11744 (2016).

[6] J. Lu, C. Qiu, L. Ye, X. Fan, M. Ke, F. Zhang, and Z. Liu, Observation of topological valley transport of sound in sonic crystals, Nat. Phys. **13**, 369 (2017).

[7] S. H. Mousavi, A. B. Khanikaev, and Z. Wang, Topologically protected elastic waves in phononic metamaterials, Nat. Commun. **6**, 8682 (2015).

[8] K. v. Klitzing, G. Dorda, and M. Pepper, New Method for High-Accuracy Determination of the Fine-Structure Constant Based on Quantized Hall Resistance, Phys. Rev. Lett. **45**, 494 (1980).

[9] D. J. Thouless, M. Kohmoto, M. P. Nightingale, and M. den Nijs, Quantized Hall Conductance in a Two-Dimensional Periodic Potential, Phys. Rev. Lett. **49**, 405 (1982).

[10] E. Prodan and C. Prodan, Topological Phonon Modes and Their Role in Dynamic Instability of Microtubules, Phys. Rev. Lett. **103**, 248101 (2009).

[11] P. Wang, L. Lu, and K. Bertoldi, Topological Phononic Crystals with One-Way Elastic Edge Waves, Phys. Rev. Lett. **115**, 104302 (2015).

[12] L. M. Nash, D. Kleckner, A. Read, V. Vitelli, A. M. Turner, and William TM Irvine, Topological mechanics of gyroscopic metamaterials, Proc. Natl. Acad. Sci. USA **112**, 14495 (2015).

[13] A. Souslov, B. C. Van Zuiden, D. Bartolo, and V. Vitelli, Topological sound in active-liquid metamaterials, Nat. Phys. **13**, 1091 (2017).

[14] N. P. Mitchell, L. M. Nash, D. Hexner, A. M. Turner, and William TM Irvine, Amorphous topological insulators constructed from random point sets, Nat. Phys. **14**, 380 (2018).

[15] H. Chen, L. Yao, H Nassar, and G. L. Huang, Mechanical quantum hall effect in time-modulated elastic materials, Phys. Rev. Appl. **11**, 044029 (2019).

[16] R. Süsstrunk and S. D. Huber, Observation of phononic helical edge states in a mechanical topological insulator, Science **349**, 47 (2015).

[17] R. K. Pal, M. Schaeffer, and M. Ruzzene, Helical edge states and topological phase transitions in phononic systems using bilayered lattices, J. Appl. Phys. **119**, 084305 (2016).

[18] H. Chen, H. Nassar, A. N. Norris, G. K. Hu, and G. L. Huang, Elastic quantum spin hall effect in kagome lattices, Phys. Rev. B **98**, 094302 (2018).

[19] R. Chaunsali, C.-W. Chen, and J. Yang, Subwavelength and directional control of flexural waves in zone-folding induced topological plates, Phys. Rev. B **97**, 054307 (2018).

[20] M. Miniaci, R. K. Pal, B. Morvan, and M. Ruzzene, Experimental Observation of Topologically Protected Helical Edge Modes in Patterned Elastic Plates, Phys. Rev. X **8**, 031074 (2018).

[21] R. K. Pal and M. Ruzzene, Edge waves in plates with resonators: An elastic analog of the quantum valley hall effect, New J. Phys. **19**, 025001 (2017).

[22] J. Vila, R. K. Pal, and M. Ruzzene, Observation of topological valley modes in an elastic hexagonal lattice, Phys. Rev. B **96**, 134307 (2017).

[23] T.-W. Liu and F. Semperlotti, Tunable acoustic valley–hall edge states in reconfigurable phononic elastic waveguides, Phys. Rev. Appl. **9**, 014001 (2018).

[24] T.-W. Liu and F. Semperlotti, Experimental evidence of robust acoustic valley hall edge states in a nonresonant topological elastic waveguide, Phys. Rev. Appl. **11**, 014040 (2019).

[25] X.-L. Qi, T. L. Hughes, and S.-C. Zhang, Topological field theory of time-reversal invariant insulators, Phys. Rev. B **78**, 195424 (2008).

[26] Y. E. Kraus and O. Zilberberg, Quasiperiodicity and topology transcend dimensions, Nat. Phys. **12**, 624 (2016).

[27] T. Ozawa, H. M. Price, N. Goldman, O. Zilberberg, and I. Carusotto, Synthetic dimensions in integrated photonics: From optical isolation to four-dimensional quantum hall physics, Phys. Rev. A **93**, 043827 (2016).

[28] C. H. Lee, Y. Wang, Y. Chen, and X. Zhang, Electromagnetic response of quantum hall systems in dimensions five and six and beyond, Phys. Rev. B **98**, 094434 (2018).

[29] V. M. M. Alvarez and M. D. Coutinho-Filho, Edge states in trimer lattices, Phys. Rev. A **99**, 013833 (2019).

[30] Y. E. Kraus, Y. Lahini, Z. Ringel, M. Verbin, and O. Zilberberg, Topological States and Adiabatic Pumping in Quasicrystals, Phys. Rev. Lett. **109**, 106402 (2012).

[31] D. J. Apigo, W. Cheng, K. F. Dobiszewski, E. Prodan, and C. Prodan, Observation of Topological Edge Modes in a Quasiperiodic Acoustic Waveguide, Phys. Rev. Lett. **122**, 095501 (2019).

[32] X. Ni, K. Chen, M. Weiner, D. J. Apigo, C. Prodan, A. Alù, E. Prodan, and A. B. Khanikaev, Observation of hofstadter butterfly and topological edge states in reconfigurable quasiperiodic acoustic crystals, Commun. Phys. **2**, 55 (2019).

[33] D. J. Apigo, K. Qian, C. Prodan, and E. Prodan, Topological edge modes by smart patterning, Phys. Rev. Mater. **2**, 124203 (2018).

[34] M. I. N. Rosa, R. K. Pal, J. R. F. Arruda, and M. Ruzzene, Edge States and Topological Pumping in Spatially Modulated Elastic Lattices, Phys. Rev. Lett. **123**, 034301 (2019).

[35] R. K. Pal, M. I. N. Rosa, and M. Ruzzene, Topological bands and localized vibration modes in quasiperiodic beams, New J. Phys. **21**, 093017 (2019).

[36] P. G. Harper, Single band motion of conduction electrons in a uniform magnetic field, Proc. Phys. Soc. A **68**, 874 (1955).

[37] S. Aubry and G. André, Analyticity breaking and anderson localization in incommensurate lattices, Ann. Isr. Phys. Soc **3**, 18 (1980).

[38] O. Zilberberg, S. Huang, J. Guglielmon, M. Wang, K. P. Chen, Y. E. Kraus, and M. C. Rechtsman, Photonic topological boundary pumping as a probe of 4D quantum hall physics, Nature **553**, 59 (2018).

[39] M. Lohse, C. Schweizer, H. M. Price, O. Zilberberg, and I. Bloch, Exploring 4D quantum hall physics with a 2D topological charge pump, Nature **553**, 55 (2018).

[40] I. Petrides, H. M. Price, and O. Zilberberg, Six-dimensional quantum hall effect and three-dimensional topological pumps, Phys. Rev. B **98**, 125431 (2018).

[41] M. Verbin, O. Zilberberg, Y. Lahini, Y. E. Kraus, and Y. Silberberg, Topological pumping over a photonic fibonacci quasicrystal, Phys. Rev. B **91**, 064201 (2015).

[42] S. Nakajima, T. Tomita, S. Taie, T. Ichinose, H. Ozawa, L. Wang, M. Troyer, and Y. Takahashi, Topological thouless pumping of ultracold fermions, Nat. Phys. **12**, 296 (2016).

[43] M. Lohse, C. Schweizer, O. Zilberberg, M. Aidelsburger, and I. Bloch, A thouless quantum pump with ultracold bosonic atoms in an optical superlattice, Nat. Phys. **12**, 350 (2016).

[44] I. H. Grinberg, M. Lin, C. Harris, W. A. Benalcazar, C. W. Peterson, T. L. Hughes, and G. Bahl, Robust temporal pumping in a magneto-mechanical topological insulator, Nat. Commun. **11**, 974 (2020).

[45] I. Brouzos, I. Kiorpelidis, F. K. Diakonos, and G. Theocharis, Non-adiabatic time-optimal edge mode transfer on mechanical topological chain, arXiv:1911.03375 (2019).

[46] S. Longhi, Topological pumping of edge states via adiabatic passage, Phys. Rev. B **99**, 155150 (2019).

[47] K. F. Graff, *Wave Motion in Elastic Solids* (Dover Publications Inc., New York, 2012).

[48] See Supplemental Material at http://link.aps.org/supplemental/10.1103/PhysRevB.101.094307 for more details on the simulation procedures, experimental setup and methodology, and for a video animation of the transient experimental analysis.

[49] L. Meirovitch, *Elements of vibration analysis* (McGraw–Hill, New York, 1975).

[50] Y. Hatsugai, Chern Number and Edge States in the Integer Quantum Hall Effect, Phys. Rev. Lett. **71**, 3697 (1993).

[51] T. Fukui, Y. Hatsugai, and H. Suzuki, Chern numbers in discretized brillouin zone: Efficient method of computing (spin) hall conductances, J. Phys. Soc. Jpn. **74**, 1674 (2005).

[52] H. Nassar, H. Chen, A. N. Norris, and G. L. Huang, Quantization of band tilting in modulated phononic crystals, Phys. Rev. B **97**, 014305 (2018).